

Wave–current interaction in the bottom boundary layer during storm and non-storm conditions: observations and model predictions

DAVID E. DRAKE* and DAVID A. CACCHIONE*

(Received 12 April 1991; accepted 28 August 1991)

Abstract—Bottom boundary layer measurements of current velocity profiles and bed response under combined wave and current conditions were obtained at a water depth of 145 m on the shelf off central California during December 1988. High quality logarithmic current profiles, excellent time-series bottom photographs, and a large variation in the relative strengths of the wave-induced oscillatory currents and the quasi-steady low frequency currents provided a dataset that is ideal for examining the effects of wave–current interaction near a rough boundary. During one period of 3 days that included a brief storm event, the wave-induced bottom currents ($U_{b/10}$) ranged from 2.3 to 22 cm s⁻¹ and the steady currents (U_r) ranged from 1.8 to 28.1 cm s⁻¹ at 0.18 m above the bottom; the ratio U_b/U_{18} varied from below 0.2 to more than 7. Velocity profiles were highly logarithmic ($R^2 > 0.95$) 60% of the time and 27 profiles collected at 2-h intervals had $R^2 \cong 0.994$ which allowed reliable estimates of the current shear velocity (U_{*c}) and roughness length (z_{oc}). Mean U_{*c} values had magnitudes of 0.3–2.4 cm s⁻¹ and z_{oc} , which ranged from 0.04 to 3.5 cm, was strongly correlated to the U_b/U_{18} ratio. Drag coefficients ($C_D = \tau_c/\rho U_{100}^2$) ranged from about 2.5×10^{-3} – 12×10^{-3} in direct response to the wave–current variation; the use of a constant C_D of 3×10^{-3} for steady flow over a rough bed would have underpredicted the shear stress by up to four times during the storm event. The large z_{oc} and U_{*c} values cannot be explained by changes in the carefully-observed, small (<1 cm) physical bed roughness elements that covered the mud-rich study site. A side-scan sonar site survey also eliminated the possibility of flow disturbance by larger upstream topography. The observations clearly demonstrate the importance of wave–current interaction near a rough boundary. Comparison of the observations with results of the combined flow models of Grant and Madsen and Glenn show the models provide good predictions of U_{*c} and z_{oc} when the waves are characterized by either $H_{1/3}$ or $H_{1/10}$.

INTRODUCTION

PREDICTIVE models of currents and sediment transport on continental shelves require a reliable means of computing boundary roughness and the bed and current shear stress values. This task is complicated by the dynamical effect of wave-induced turbulence near the sea floor and by the need to evaluate changes in bed roughness elements and scales that may be caused by strong currents, biological activities, and episodes of erosion and deposition.

The bottom boundary layer models developed by SMITH (1977) and by GRANT and MADSEN (1979) predict nonlinear enhancement of the wave and current shear stresses in a combined flow over a hydrodynamically-rough sea floor. Both of these models showed

*U.S. Geological Survey, Menlo Park, CA 94025, U.S.A.

early promise in comparison with a limited set of velocity profile observations made in Norton Sound, Alaska (CACCHIONE and DRAKE, 1982; WIBERG and SMITH, 1983). More recently, data collected on the California shelf (GRANT *et al.*, 1984; CACCHIONE *et al.*, 1987), on the Nova Scotian shelf of Canada (HUNTLEY and HAZEN, 1988), and, in Marsden Bay, England (GREEN *et al.*, 1990) have been used to examine the predictions of the GRANT and MADSEN (hereafter GM79) combined flow model. In each case the GM79 model has performed well and these studies have supported the importance of wave-current interaction. However, the experiments to date have either covered only a limited range of wave-current speeds (HUNTLEY and HAZEN, 1988) or the physical bed roughness scales and their temporal variation have not been well known (CACCHIONE and DRAKE, 1982; CACCHIONE *et al.*, 1987; WIBERG and SMITH, 1983; GREEN *et al.*, 1990). Thus, the experiments of HUNTLEY and HAZEN (1988) and GRANT *et al.* (1984) verified the model results for the current shear (U_{*c}) during tranquil (subthreshold) flows over fixed bed roughness elements. The other experiments, which included times when considerable sediment transport was taking place and presumably bedforms were formed, were unable to adequately monitor the changes in the local bed roughness. Because the dynamics of the bottom boundary layer (bb1) are related to the bed roughness scales as well as to the wave-induced turbulent interactions which produce an apparent additional roughness for the mean current above the wave boundary layer, knowledge of the sizes and distribution of physical roughness elements is important to model verification. This problem takes on added importance in models of sediment transport because of the need to properly specify the contribution of the wave oscillatory currents to the bed shear stress (GRANT and MADSEN, 1986; GREEN *et al.*, 1990) which initiates erosion and also the need to specify the current shear velocity (U_{*c}) as input to the computation of the equilibrium distribution of suspended particles in the boundary layer (GLENN and GRANT, 1987). As discussed by GREEN *et al.* (1990), the wave oscillatory currents (U_b) have been parameterized quite differently in the experiments described above. HUNTLEY and HAZEN (1988) and GREEN *et al.* (1990) used "significant-wave" statistics ($H_{1/3}$ and $U_{b1/3}$); LARSEN *et al.* (1981) and DRAKE and CACCHIONE (1986) used averages of the one-tenth largest waves ($U_{b1/10}$) and, GRANT *et al.* (1984) used the maximum wave height recorded in 10-min burst pressure samples. Although these studies clearly support the theory of enhanced current shear and apparent boundary roughness by wave-current interaction, the specific choice of wave parameters to use in the model for sediment transport estimates remains unclear. Because $U_{b(\max)}$ will generally exceed $U_{b1/3}$ by 50% in an open-shelf wave field, and the bed shear stress that drives sediment transport varies as U_b^2 , wave characterization is an important issue.

Our objective in this paper is to analyse boundary layer current, wave and suspended sediment measurements obtained during the winter of 1988/1989 with a GEOPROBE tripod system (CACCHIONE and DRAKE, 1979, 1990) on the outer shelf off central California (Fig. 1) in terms of the combined-flow models of GRANT and MADSEN (1979), GLENN (1983), and GLENN and GRANT (1987). The dataset is ideally suited to this purpose because the occurrence of a brief storm event on 21–22 December 1988 produced a large range in the relative strengths of the wave-induced and mean bottom currents. Pre-storm and post-storm bed roughness scales and storm-induced bedform changes were carefully determined using side-scan sonar surveys, stereo 70 mm photography (from shipboard) and time-lapse 35 mm photography (mounted on GEOPROBE). The mean horizontal velocity profiles within 1.2 m of the bed were highly logarithmic more than 60% of the time,

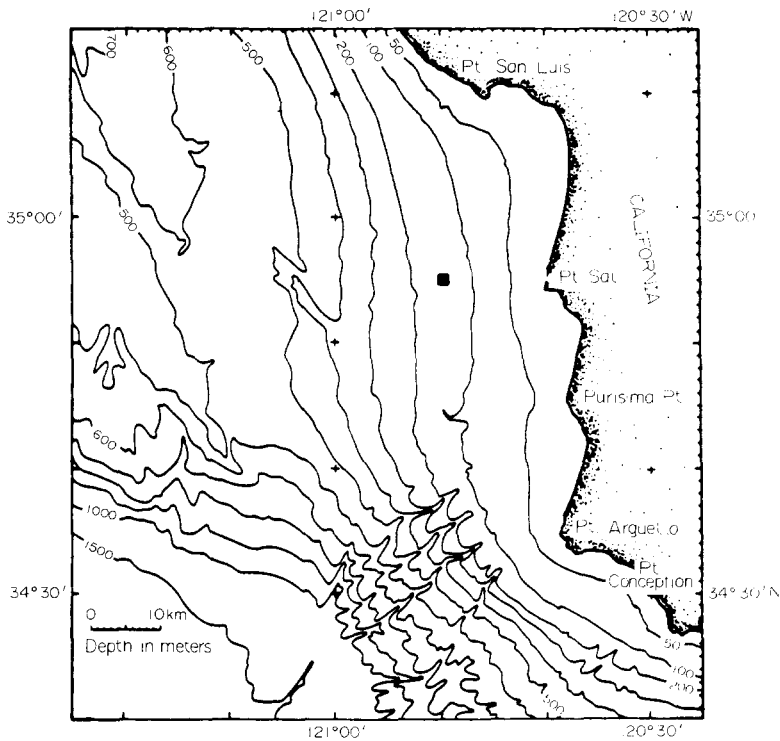


Fig. 1. The location of the GEOPROBE tripod at a depth of 145 m on the outer shelf off Point Sal, California is shown by the solid square. The tripod was deployed on 8 December 1988 and recovered on 22 February 1989.

which allowed good estimates of the current shear (U_{*c}) and apparent roughness length (z_{oc}) using the von Karman-Prandtl “law-of-the-wall” velocity relationship for rough-turbulent flow.

The data show a direct correspondence between the observed apparent roughness (z_{oc}) and the ratio of wave to current speeds (U_b/U_r), and the predictions of the combined flow model of GM79 are in excellent agreement with observed values of U_{*c} and z_{oc} when either $U_{b1/3}$ or $U_{b1/10}$ are used to describe the waves. Predictions of suspended matter resuspension and bbl concentrations by the model of GLENN and GRANT (1987) with $U_{b1/10}$, accurately predict the initiation of motion but overestimate concentrations at 1 mab by factors of 2–5; cohesiveness of the mud-rich bed offers an explanation for this discrepancy.

SITE SURVEYS, DATA COLLECTION AND ANALYSIS

The GEOPROBE tripod was deployed at a water depth of 145 m on the outer shelf off Point Sal, California in December 1988 (Fig. 1) following a site survey with side-scan sonar and 3.5 kHz seismic reflection profiling systems, a 70-mm bottom-tripping camera, and sediment sampling with a box corer. This part of the central California shelf is covered by inorganic modern, sandy clayey silt (sand/silt/clay = 20/65/15) derived from local river

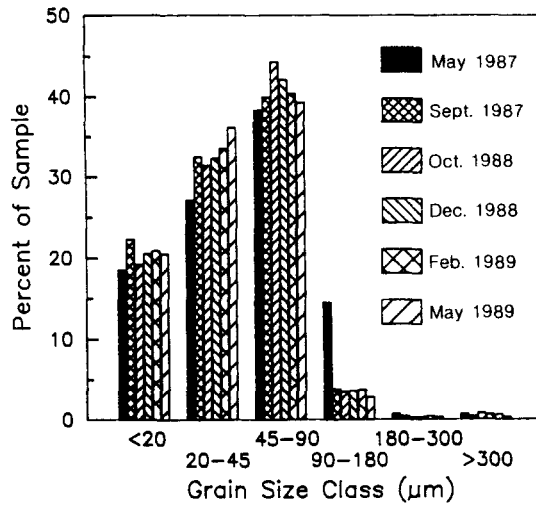


Fig. 2. Particle-size distribution of the surficial sediment layer (0–2 mm) in six box cores recovered by C. A. Butman during the CAMP field program. Note that the size interval is uneven; the mean diameter is in the coarse silt size grade at about 0.004 cm.

sources. The modal grain size in the medium silt range (0.004 cm) and the relatively poor sorting suggest a predominantly low-energy environment of deposition (Fig. 2). Box core sediments from the site are intensely mixed by the burrowing of worms and brittle stars and the sea floor character revealed by bottom photographs attests to the general dominance of the benthos in producing bottom topography (Fig. 3).

The side-scan sonar system used in this survey is capable of resolving bed features with vertical dimensions larger than 10–15 cm. Large current ripples in coarse sand are easily resolved, but the smaller (1–5 cm high) ripples that can develop on fine sand and coarse silt substrates cannot be detected with this system. Several passes through our study site at 145 m revealed no natural bedforms large enough to be detected. However, as shown in Fig. 4, the bottom is commonly disrupted by long, linear gouges that we judge to be several decimeters deep and which trend obliquely across the shelf edge. This region is an important commercial fishing ground and the linear gouges are produced by bottom trawling. We took precautions to avoid deploying the GEOPROBE within 500 m of any fresh gouges and we deployed a pair of large surface guard buoys to divert trawlers during the experiment.

The bed topography here is homogeneous and best studied using photographic methods. Prior to GEOPROBE deployment, 70-mm stereo photographs were obtained on a 1-km transect through the site by K. Briggs and R. Ray of the Naval Ocean Research and Development Administration (NORDA). The photographs, of which Fig. 3 is representative, reveal a mottled sediment surface covered by low mounds and depressions produced by worms, brittle stars, and bottom fish. Analysis of a number of these photographs (covering about 12 m²) shows that there were no bed roughness elements larger than the mounds and burrows shown in Fig. 3. In effect, the sea floor within 1 km of the GEOPROBE can be considered to be a flat surface covered with closely-spaced mounds and depressions with the relief ranging from a few mm up to about 2 cm.



Fig. 3. Small mounds and burrows, produced by an abundant benthos dominated by brittle stars and polychaete worms, were typical of the sea floor roughness elements near the GEOPROBE tripod site. The dark crosses on the photograph, which was taken on 9 December 1988, are 25 cm apart. Physical bed roughness was homogeneous and the heights of the various elements were no more than 2 cm. Photograph courtesy of Kevin Briggs, NORDA.

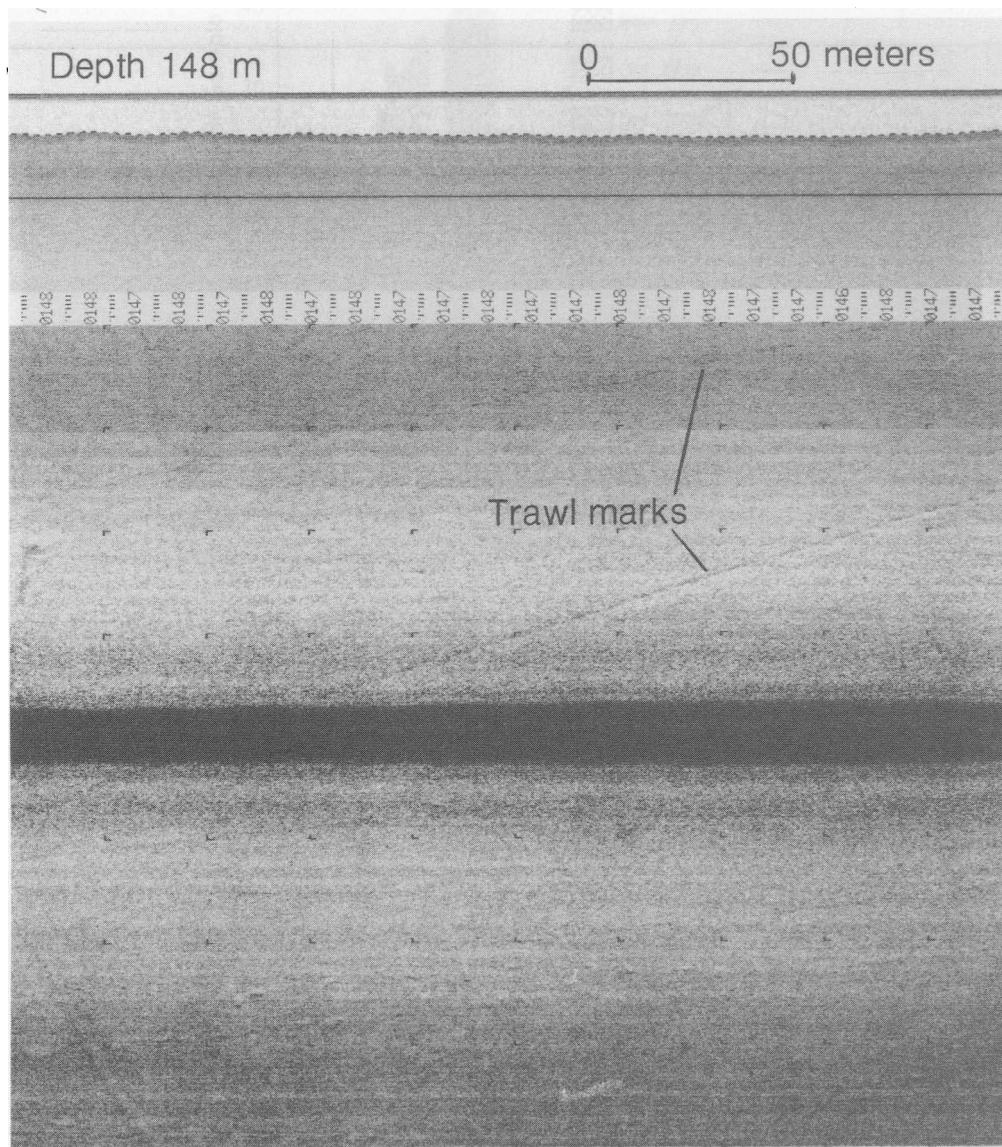


Fig. 4. Side-scan sonograph obtained during the pre-deployment site survey. The image reveals trawl marks caused by commercial fishing activity on an otherwise flat and featureless sea floor.

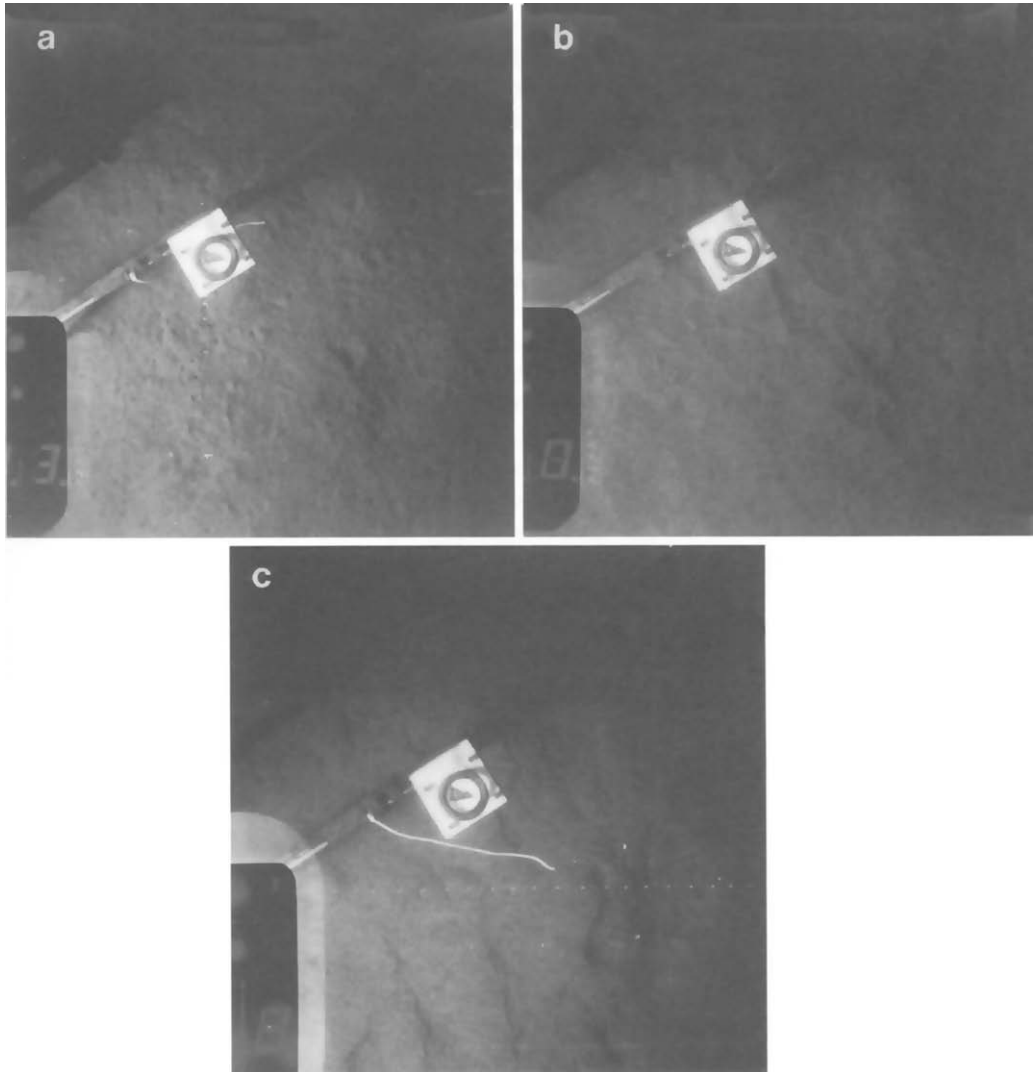


Fig. 8. Photographs of the sea floor inside the GEOPROBE tripod frame during 21–24 December; (a) the bed prior to the storm was covered by small biological roughness elements in good agreement with the low z_{oc} values (about 0.08 cm) observed when wave to current ratios were small (see Table 3); (b) small wave ripples with lengths of 5–10 cm and maximum amplitudes of 0.5 cm were produced by the strong wave action on 22 December; (c) strong ($>25 \text{ cm s}^{-1}$) mean current pulses on 22 December and 24 December (see Fig. 6) produced small-amplitude current ripples which conformed to expected dimensions for the coarse silt sediment at this site. These ripples did not cause a significant increase in the physical bed roughness scale (z_o) or in the apparent roughness length, z_{oc} .

Polychaetes (worms) and Ophiroids (brittle stars) are common on this shelf. The brittle stars, in particular, produce small conical depressions where their arms extend above the sea floor for food gathering. Despite an excellent series of photographs, it is difficult to accurately measure amplitudes of the smallest, biologically-produced topography. Using scattered clam shells and the numerous exposed brittle star arms for scaling, we estimate the average height and spacing of the roughness elements to be about 0.6 and 7 cm, respectively. Our assessment of the physical roughness length (z_0) suggested by the sea floor photographs and also by the current profiles during times of low wave speeds will be discussed later.

The regional flow field near the seafloor on the outer part of the California shelf in this area is typically composed of a low-frequency current directed toward the north-northwest (the so-called "poleward undercurrent") at average speeds of 5–10 cm s⁻¹, semidiurnal and diurnal tidal currents of up to 15 cm s⁻¹, along with a variable but generally weak contribution by wind-driven currents (Fig. 5). The average current speed over the 60-day deployment at 18 cm above bottom on GEOPROBE was 7.7 cm s⁻¹.

Peak flows reached nearly 30 cm s⁻¹ on 22–24 December. Wave-generated oscillatory currents are usually weak (<5 cm s⁻¹) at depths of 145 m and only surface waves with periods greater than about 12 s could reasonably be expected to cause significant currents at the GEOPROBE site. Through much of the year the waves are too small to disturb the sea floor here, but swell generated by northeast Pacific storms in the winter commonly enters the area with periods of 12–18 s and heights of 3–5 m (Fig. 5); bottom orbital currents at 145 m during these events will exceed 20 cm s⁻¹, which is above threshold for erosion of silt and fine sand. The resulting wave and current variations are ideal for examining the combined-flow boundary layer model.

Bottom boundary layer measurements

The GEOPROBE tripod was equipped with four spherical electromagnetic current meters (EMCM) to measure two orthogonal components of the horizontal flow at heights of 18, 52, 85 and 118 cm above the sea floor. The EMCM's and a *Paroscientific* quartz crystal pressure sensor were sampled in a "burst" mode at a rate of 0.5 Hz for 10 min every 2 h (Table 1). Burst samples provided information on the wave-generated oscillatory currents and pressure variations. They were also averaged to evaluate the "steady", horizontal currents, and tidal, and subtidal pressure variations. Wave periods were determined by the method of "zero crossings" in the pressure record following subtraction of the burst mean pressure. Wave-generated bottom oscillatory currents were depicted in two ways; as the average of the one-third largest waves ($U_{b1/3}$); and as the average of the one-tenth largest waves ($U_{b1/10}$). $H_{1/3}$ and $H_{1/10}$ were estimated as (BRETSCHNEIDER, 1966):

$$H_{1/3} = 1.6\bar{H} \quad \text{and} \quad H_{1/10} = 1.27H_{1/3}.$$

The GEOPROBE also measured water temperature at 2 and 0.3 m above the bottom once during each burst in order to check for boundary layer stratification that would effect the velocity profiles. We found no evidence for thermal stratification and we have assumed there was no density stratification caused by salinity gradients. Some support for this assumption comes from hydrographic data obtained from shipboard with profiling salinity-temperature-depth sensors during the deployment and recovery phases of the

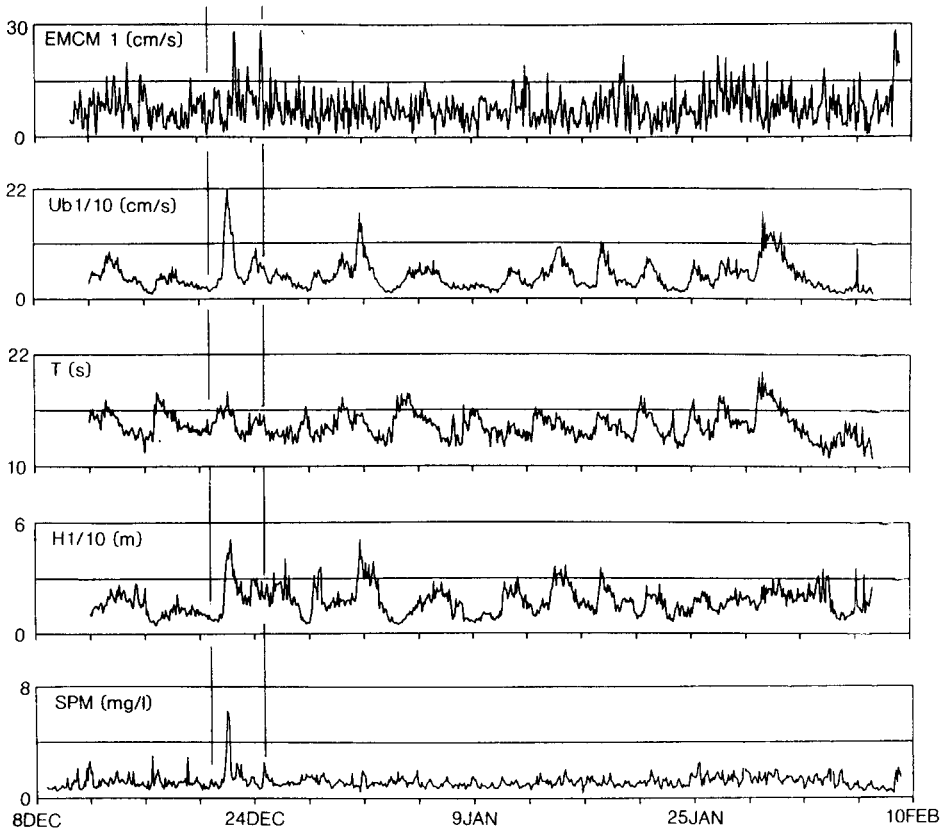


Fig. 5. Time-series of GEOPROBE data collected during 8 December 1988–8 February 1989. The top panel presents the burst-averaged horizontal current speed (cm s^{-1}) at 18 cm above the sea floor. The center three panels show surface wave parameters (period and height) and the average bottom orbital velocity of the 10% largest waves ($U_{b1/10}$). The bottom panel presents suspended particulate matter (SPM) concentration estimates (in mg l^{-1}) based on transmissometer measurements at 98 cm above the sea floor. The part of the record which brackets the storm event, 21–25 December, and is examined in detail, is identified by the light vertical lines.

Table 1. Geoprobe location and sampling data

| Location | Depth (m) | Burst sampling | | |
|-------------------------|--------------|-------------------|-------------|-------------------|
| | | Interval (min) | Rate (s) | Duration (min) |
| 34°54.9'N 120°49.8'W | 145 | 120 | 2 | 10 |

experiment. The profiles showed a well-mixed bottom layer 5–20 m thick at our outer shelf and upper slope stations.

Light-beam transmission at 0.98 m above bottom was measured once during each burst sequence with a *Sea Tech Inc.* light-emitting-diode (LED), 25-cm pathlength transmissometer. This sensor uses red light at 660 μm to avoid significant attenuation (absorption) by dissolved organic matter. The LED transmission data were converted to beam attenuation (c) per meter according to $c = -\ln T/r$, where T is transmission and r is the pathlength in meters. Our interest is in the concentration of suspended particulate matter (SPM) and, therefore, we have calibrated the beam attenuation values of the transmissometer using both laboratory data and analyses of the particle content of water samples collected from shipboard in the survey region. More than 50 samples were used to define the relation between SPM and beam attenuation. The major source of error in the relationships is variation in particle sizes which can cause light attenuation differences at constant concentrations (BAKER and LAVELLE, 1984). Calibration curves that are developed for specific experiments and measurement sites (i.e. substrate types) help to reduce this error, but it cannot be completely eliminated without information on the particle sizes in suspension. We did not collect water samples on the GEOPROBE for grain size analysis, and thus our estimates of SPM concentration could be in error by ± 50 –100%, particularly during storm events when the sea floor is eroded and particle sizes should vary.

Analysis of current profiles

The EMCM sensors at 18, 85 and 118 cm ab functioned properly throughout the experiment allowing estimates of the boundary shear velocity (U_{*c}) and the roughness length (z_{oc}) for the mean current above the wave boundary layer, whenever the burst-averaged horizontal flow conformed to the logarithmic velocity law for steady, rough-turbulent flow

$$U_r = \frac{U_{*c}}{\kappa} \ln \left(\frac{z}{z_{oc}} \right) \quad (1)$$

where κ is von Karman's constant (equal to 0.41). To make the best possible estimates of U_{*c} and z_{oc} using the mean velocity profile method, one needs to ensure that:

- (1) the boundary layer is well-mixed and not stratified by temperature, salinity, or suspended sediment;
- (2) the speed measurements are sampled for a length of time that is sufficient to properly evaluate the characteristics of the wave-induced currents, but not so long as to suffer from nonstationary flow;
- (3) the heights of the sensors above the bottom are known;
- (4) the correlation coefficient (R) that describes the degree to which the burst-averaged speeds conform to the log velocity profile [equation (1)] is high enough to lend confidence to the estimates.

As noted above, temperature data were obtained to assess bbl stratification by temperature and salinity. Suspended matter at sufficiently large concentrations and gradients can reduce turbulence and produce density stratification that causes the mean velocity profiles to deviate from the neutral log profile described by equation (1) (GLENN, 1983). As discussed by GLENN and GRANT (1987), both large SPM concentrations and a

vertical gradient are required to stratify the bbl. Thus a large concentration of a uniformly-mixed, fine-grained material (e.g. clay) will not stratify the flow, whereas a strong vertical gradient in concentration (such as might be produced by relatively large silt and sand particles) will cause important turbulence damping and “breaks” or bends in the velocity profile.

The order of magnitude of SPM needed to produce significant effects on the velocity profiles for various particles (i.e. a range of grain settling velocities, w_s), can be estimated using an expression for the gradient Richardson number (HEATHERSHAW, 1979):

$$R_i \cong \frac{w_s \kappa z g C}{U_{*c}^3 \rho} \left(1 - \frac{\rho}{\rho_s} \right). \quad (2)$$

Atmospheric boundary layers are considered neutrally buoyant when $R_i \leq 0.03$. Taking the settling velocity $w_s = 0.2 \text{ cm s}^{-1}$ for coarse silt, $z = 50 \text{ cm}$, and $U_{*c} = 1 \text{ cm s}^{-1}$, equation (2) indicates a detectable deviation of the velocity profile will occur when C exceeds about 30 mg l^{-1} . However, a 5% change in U_{*c} requires concentrations of coarse silt of about $200\text{--}300 \text{ mg l}^{-1}$. Since the highest SPM concentration measured by the Sea Tech transmissometer at 98 cm ab during the present experiment was of the order of 10 mg l^{-1} we have assumed that the gravitational stability imparted by suspended sediment was always negligible.

LESHT (1980) and GRANT *et al.* (1984) have addressed the question of the duration of sampling (Δt) that is needed to produce stable estimates of U_* and z_0 , and also reliable wave characterization. LESHT (1980) found no significant improvement in the fit of mean current data to equation (1) when $\Delta t \geq 20(z/U_z)$; for our dataset the burst sample duration of 10 min always exceeded Lesht’s criterion. Proper sampling of the surface wave field depends upon the expected individual wave periods (T) and on the typical period of wave groups (beating). At a depth of 145 m surface waves with $T < 12\text{s}$ will not be significant flow generators (using the rough criterion that the wave “feels” bottom when $h \leq 0.5L$). Thus a sample rate of 0.5 Hz adequately sampled each wave. Wave groups with periods of about 2–3 min are evident in our 10-min burst records; our analysis of several of these records indicates poor characterization of the average and the significant wave heights and current velocities when the sample interval is less than about 4–6 min. Our 10-min interval is assumed to have produced stable and accurate estimates of both the mean horizontal currents and the wave-induced oscillatory currents and average periods.

Current-sensor heights above the deck of the ship were measured before and after the experiment and these values served as the nominal heights (z) above the sea floor. In order to determine the best final sensor elevations, which would account for possible sinkage of the tripod into the muddy sediment, we analysed the R^2 correlations of burst-averaged velocities to equation (1) using settlement amounts of 0, 2, 5 and 10 cm. The highest average R^2 values were found for either 0 or 2 cm settlement, whereas considerably lower regression coefficients were found for settlement of more than 2 cm. Because no clear improvement in the fit of the velocity profiles to equation (1) could be found by sinking the tripod, we have not adjusted the EMCM heights.

Finally, it is critically important to use velocity profiles that have suitably high correlation coefficients to compare with the predictions of GM79 (WIBERG and SMITH, 1983; GROSS and NOWELL, 1983; GRANT *et al.*, 1984). The confidence interval on shear velocity estimates depends on the regression coefficient (R), the number of current sensors, and their vertical placement. With three current sensors the error band is

unacceptably large if R is less than 0.997 ($R^2 = 0.994$). To keep the error bars on U_{*c} estimates to $\pm 25\%$ or less at the 90% confidence level, a minimum R value of 0.998 is required. Although we will present U_{*c} and z_{oc} estimates for $R < 0.998$, we have used only profiles with $R \geq 0.998$ for our rigorous comparison with the model predictions.

RESULTS

Velocity profiles

Mean current speed at 18 cm ab, surface wave heights and the associated bottom oscillatory currents (expressed as $H_{1/10}$ and $U_{b1/10}$, respectively), average wave period, and suspended particulate matter concentration based on light beam attenuation at 98 cm ab are presented for the entire experiment in Fig. 5. Although shelf currents and waves in the winter season can be larger than at other times on this shelf, the relatively great depth of this site diminishes the effect of storm winds and waves. In general, both the wave-induced and the burst-averaged currents were below 10 cm s^{-1} during most of the experiment. The sparseness of large bed shear stress events and associated erosion of even this fine-grained mud substrate is clearly reflected by the uneventful suspended sediment record (Fig. 5). The optical data shows that variation in SPM was typically less than 1 mg l^{-1} over days to weeks. Only one strong pulse of SPM, estimated to have peaked at about 6 mg l^{-1} at 98 cm ab early on 22 December 1988, was clearly associated with the most energetic wave oscillatory currents of the season (Figs 5 and 6). Other storm wave events on 31 December 1988 and late January 1989 produced only small to undetectable increases in SPM.

Our analysis of the mean current speeds measured every 2 h shows that $>50\%$ of the velocity profiles had $R \geq 0.9$ when fitted to equation (1). While these profiles would be considered logarithmic, the error bars on U_* estimates are excessively large ($>\pm 25\%$) for $R \leq 0.998$. To develop confidence in the accuracy of predictions made by the model, we have analysed a subset of velocity profiles for which $R > 0.998$. Fortunately, we obtained 27 suitable profiles during the pre-storm, storm and post-storm interval of 21–24 December 1988 (Fig. 6). Conditions during this time period were ideal for our objectives; wave $U_{b1/10}$ to U_{18} ratios exhibited an extreme range of 0.17–8.5, the bed was photographed successfully every 4 h, and both the photographs and the light attenuation data show that the threshold for local sediment motion was exceeded and ripples were formed. Temperature data during this time show no evidence for stratification of the bbl and the very low concentrations of suspended matter (less than 10 mg l^{-1}) would have had no detectable influence on the flow dynamics.

The results of our velocity profile analysis are given in Table 2, and time-series of “observed” U_{*c} , z_{oc} , and the boundary drag coefficients are plotted in Fig. 7. The measured profiles yield average U_{*c} and z_{oc} estimates of about 1.0 cm s^{-1} and 0.50 cm , respectively, and these are large relative to the expected values for steady currents over the observed sea floor (Figs 2 and 8). Drag coefficients, computed as $C_D = U_{*c}^2 / \rho U_{100}^2$, for the measured mean flows at 1 m ranged from about 2.5×10^{-3} when U_b/U_r was small to almost 12×10^{-3} when U_b/U_r was high (Fig. 7; Table 2). The usual C_D values of 1.5×10^{-3} for a “smooth” bottom and 3.0×10^{-3} for “rough” bottom types (STERNBERG, 1972), which are used by modelers of shelf currents, are substantially lower than many of the observed drag coefficients.

The large shear velocities and drag coefficients were caused by large increases in the boundary roughness length (z_{oc}) experienced by the current, particularly during

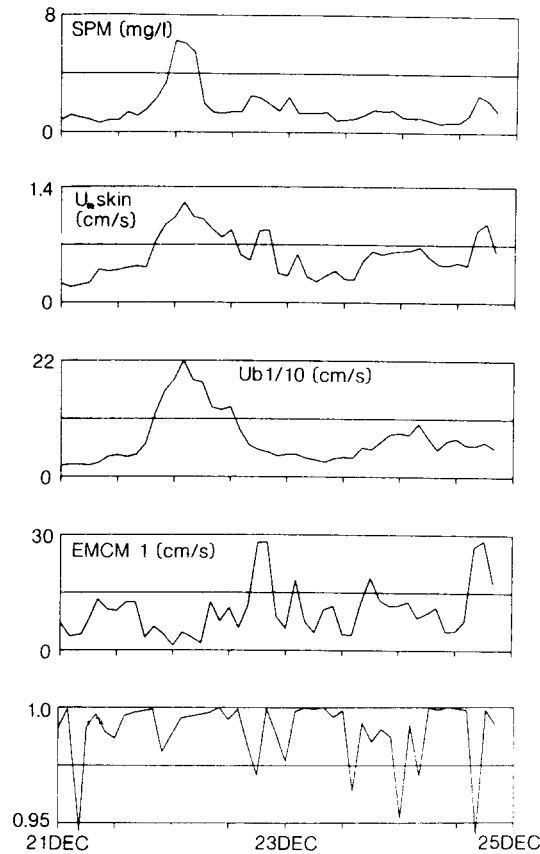


Fig. 6. Current, wave, and suspended matter data during 21–25 December 1988. The lower panel shows the regression coefficient (R^2) for all of the mean current profiles fitted to the logarithmic law-of-the-wall, $\bar{U} = (U_* / \kappa) \ln(z/z_0)$. The second panel presents an estimate of the shear velocity (U_*) applied to the silt grains based on the combined-flow, bottom boundary layer model of GLENN (1983).

0000 hours to 0600 hours on 22 December when the waves were large and the steady current was relatively low (Figs 7 and 9). The large z_{oc} , C_D , and U_{*c} values observed during that time of large storm waves is precisely that which is predicted by combined flow theories. However, it is also possible that the observed roughness increase was caused by a major change in the physical roughness due to storm-wave production of large bedforms. The issue of unknown changes in the physical k_b during the course of an experiment has hampered several previous studies of flow interaction. Fortunately, the beam attenuation data, the bottom photographs and the post-storm current profiles collected by GEOPROBE in the present study allow a definitive conclusion on this matter. First, after a pre-storm interval when $z_{oc} \approx 0.1$ cm (Table 2, Fig. 7), the measured z_{oc} reached values of 2.5–3.5 cm during the storm suggesting an equivalent physical roughness length of about $k_b = 30z_0 = 90$ cm. The bottom photographs obtained immediately after the peak of the storm (Fig. 8) reveal small wave-formed ripples with maximum heights of about 1 cm and wave lengths of 7–10 cm; there is no evidence in the photographs for bedforms of the

Table 2. Boundary layer observations and model results

| Profile No. | Time | Observations | | | | | | | | | | Model | | | | | | | | | | | |
|-------------|------|--------------------------------|-------|--------------------------------|---------------|----------------------------|---------------------------------|------|----------------------------------|------------|--------------------------------|---------------|---------------------------------|------------|-----|-----------------------------------|------------|--------------------------------|---------------|---------------------------------|------------|-----|-----|
| | | U_{18} (cm s ⁻¹) | R^2 | U_{re} (cm s ⁻¹) | z_{re} (cm) | C_D ($\times 10^{-3}$) | C_{100} (mg l ⁻¹) | Bed† | $U_{b1/3}$ (cm s ⁻¹) | A_b (cm) | U_{re} (cm s ⁻¹) | z_{re} (cm) | C_{100} (mg l ⁻¹) | k_b (cm) | Bed | $U_{b1/10}$ (cm s ⁻¹) | A_b (cm) | U_{re} (cm s ⁻¹) | z_{re} (cm) | C_{100} (mg l ⁻¹) | k_b (cm) | Bed | |
| 21DEC | | | | | | | | | | | | | | | | | | | | | | | |
| 1 | 0200 | 3.6 | 0.999 | 0.44 | 0.66 | 6.0 | 1.3 | B | 2.0 | 4.6 | 0.34 | 0.28 | — | 2.6 | — | 2.3 | 5.4 | 0.35 | 0.31 | — | 2.6 | — | 2.6 |
| 2 | 0800 | 13.3 | 0.997 | 0.84 | 0.04 | 2.4 | 1.5 | B | 1.9 | 4.9 | 1.05 | 0.11 | — | 2.6 | — | 2.7 | 6.9 | 1.08 | 0.13 | — | 2.6 | — | 2.6 |
| 3 | 1400 | 12.5 | 0.996 | 1.01 | 0.12 | 3.4 | 1.7 | B | 3.2 | 8.5 | 1.04 | 0.15 | — | 2.6 | — | 3.7 | 9.8 | 1.06 | 0.16 | — | 2.6 | — | 2.6 |
| 4 | 1600 | 12.5 | 0.997 | 1.02 | 0.13 | 3.5 | 1.4 | B | 3.4 | 8.5 | 1.05 | 0.15 | — | 2.6 | — | 4.2 | 10.5 | 1.08 | 0.17 | — | 2.6 | — | 2.6 |
| 5 | 1800 | 3.3 | 0.994 | 0.30 | 0.22 | 3.2 | 1.9 | B | 4.8 | 11.5 | 0.39 | 0.63 | — | 2.6 | — | 6.4 | 15.4 | 0.43 | 0.81 | — | 2.6 | — | 2.6 |
| 6 | 2000 | 6.2 | 0.999 | 0.70 | 0.52 | 5.5 | 3.1 | B | 8.8 | 22.1 | 0.75 | 0.65 | — | 2.6 | — | 12 | 30.1 | 0.81 | 0.83 | — | 2.6 | — | 2.6 |
| 22DEC | | | | | | | | | | | | | | | | | | | | | | | |
| 7 | 0200 | 4.7 | 0.995 | 0.91 | 2.30 | 10.1 | 6.3 | WR | 17.7 | 50.7 | 0.78 | 1.67 | 1.8 | 2.6 | — | 22 | 63.0 | 0.88 | 2.12 | 20 | 2.8 | R | R |
| 8 | 0600 | 1.8 | 0.995 | 0.43 | 3.51 | 11.9 | 3.3 | WR | 14.3 | 35.3 | 0.36 | 2.38 | 0.2 | 2.6 | — | 17.9 | 44.0 | 0.39 | 2.9 | 5.7 | 2.8 | R | R |
| 9 | 0800 | 12.6 | 0.997 | 1.15 | 0.23 | 3.9 | 2.0 | B | 10.0 | 24.8 | 1.29 | 0.36 | — | 2.6 | — | 13.2 | 32.3 | 1.38 | 0.47 | 1.0 | 2.6 | — | 2.6 |
| 10 | 1000 | 7.6 | 1.000 | 0.77 | 0.35 | 4.7 | 1.6 | B | 9.8 | 25.3 | 0.89 | 0.59 | — | 2.6 | — | 12.7 | 32.7 | 0.96 | 0.77 | — | 2.6 | — | 2.6 |
| 11 | 1200 | 11.1 | 0.994 | 1.06 | 0.28 | 4.3 | 1.6 | B | 10.2 | 25.7 | 1.17 | 0.41 | — | 2.6 | — | 13.3 | 33.3 | 1.27 | 0.54 | — | 2.6 | — | 2.6 |
| 12 | 1400 | 5.8 | 0.999 | 0.57 | 0.30 | 4.0 | 1.5 | B | 6.7 | 16.2 | 0.66 | 0.53 | — | 2.6 | — | 8.8 | 21.3 | 0.71 | 0.69 | — | 2.6 | — | 2.6 |
| 13 | 1800 | 27.9 | 0.994 | 2.06 | 0.08 | 3.3 | 2.8 | CR | 4.0 | 9.2 | 2.19 | 0.11 | 2.2 | 2.6 | — | 5.1 | 11.6 | 2.22 | 0.12 | 4.0 | 2.6 | R | R |
| 14 | 2000 | 28.1 | 0.999 | 2.16 | 0.10 | 3.3 | 2.5 | CR | 3.8 | 8.2 | 2.20 | 0.11 | — | 2.6 | — | 4.7 | 10.1 | 2.23 | 0.12 | 3.2 | 2.6 | R | R |
| 23DEC | | | | | | | | | | | | | | | | | | | | | | | |
| 15 | 0200 | 18.2 | 0.998 | 1.45 | 0.12 | 3.3 | 2.0 | CR-B | 3.6 | 8.0 | 1.47 | 0.12 | — | 2.6 | — | 4.3 | 9.4 | 1.48 | 0.13 | — | 2.6 | — | 2.6 |
| 16 | 0400 | 7.6 | 0.999 | 0.81 | 0.42 | 5.0 | 2.1 | CR-B | 2.7 | 6.0 | 0.67 | 0.19 | — | 2.6 | — | 3.6 | 7.9 | 0.70 | 0.23 | — | 2.6 | — | 2.6 |
| 17 | 0600 | 4.6 | 0.999 | 0.48 | 0.39 | 4.8 | 1.4 | CR-B | 2.9 | 6.1 | 0.45 | 0.31 | — | 2.6 | — | 3.2 | 6.8 | 0.46 | 0.33 | — | 2.6 | — | 2.6 |
| 18 | 0800 | 10.6 | 1.000 | 0.92 | 0.18 | 3.8 | 1.5 | CR-B | 2.4 | 4.9 | 0.87 | 0.14 | — | 2.6 | — | 2.8 | 5.6 | 0.89 | 0.15 | — | 2.6 | — | 2.6 |
| 19 | 1000 | 11.5 | 0.995 | 0.74 | 0.05 | 2.5 | 1.4 | CR-B | 2.6 | 5.8 | 0.95 | 0.14 | — | 2.6 | — | 3.5 | 7.7 | 0.96 | 0.15 | — | 2.6 | — | 2.6 |
| 20 | 1200 | 4.1 | 0.998 | 0.46 | 0.52 | 5.4 | 1.1 | CR-B | 3.3 | 7.4 | 0.42 | 0.38 | — | 2.6 | — | 3.7 | 8.1 | 0.43 | 0.45 | — | 2.6 | — | 2.6 |
| 21 | 1600 | 12.5 | 0.994 | 1.19 | 0.17 | 4.2 | 1.3 | CR-B | 4.5 | 11.2 | 1.09 | 0.18 | — | 2.6 | — | 5.6 | 13.9 | 1.13 | 0.21 | — | 2.6 | — | 2.6 |
| 24DEC | | | | | | | | | | | | | | | | | | | | | | | |
| 22 | 0200 | 12.6 | 0.994 | 1.07 | 0.16 | 3.5 | 1.5 | CR-B | 6.4 | 15.3 | 1.16 | 0.24 | — | 2.6 | — | 8.0 | 19.2 | 1.22 | 0.29 | — | 2.6 | — | 2.6 |
| 23 | 0600 | 9.6 | 0.999 | 1.04 | 0.45 | 5.1 | 1.5 | CR-B | 6.0 | 14.2 | 0.93 | 0.29 | — | 2.6 | — | 7.4 | 17.6 | 0.98 | 0.35 | — | 2.6 | — | 2.6 |
| 24 | 0800 | 11.2 | 1.000 | 0.98 | 0.19 | 3.8 | 1.0 | CR-B | 4.1 | 9.3 | 0.98 | 0.19 | — | 2.6 | — | 5.1 | 11.7 | 1.01 | 0.22 | — | 2.6 | — | 2.6 |
| 25 | 1000 | 4.9 | 1.000 | 0.70 | 1.10 | 7.4 | 1.0 | CR-B | 5.4 | 13.5 | 0.57 | 0.57 | — | 2.6 | — | 6.9 | 17.0 | 0.61 | 0.72 | — | 2.6 | — | 2.6 |
| 26 | 1400 | 7.7 | 0.998 | 0.99 | 0.77 | 6.2 | 1.3 | CR-B | 4.8 | 11.2 | 0.75 | 0.29 | — | 2.6 | — | 6.1 | 14.2 | 0.79 | 0.37 | — | 2.6 | — | 2.6 |
| 27 | 1800 | 28.5 | 0.999 | 2.44 | 0.17 | 3.7 | 3.0 | CR-B | 5.2 | 12.8 | 2.27 | 0.12 | — | 2.6 | — | 6.6 | 16.3 | 2.32 | 0.13 | 4.8 | 2.6 | — | 2.6 |
| 28 | 2000 | 17.5 | 0.984 | 1.44 | 0.14 | 3.4 | 2.0 | CR-B | 4.4 | 9.9 | 1.45 | 0.14 | — | 2.6 | — | 5.5 | 12.2 | 1.49 | 0.16 | — | 2.6 | — | 2.6 |

† Bed roughness elements were dominated by: B, biologic mounds and burrows; WR, wave ripples; CR, current ripples; or a combination of current ripples and biologic elements, CR-B. The physical bed roughness length, $k_0 = 30z_0$.

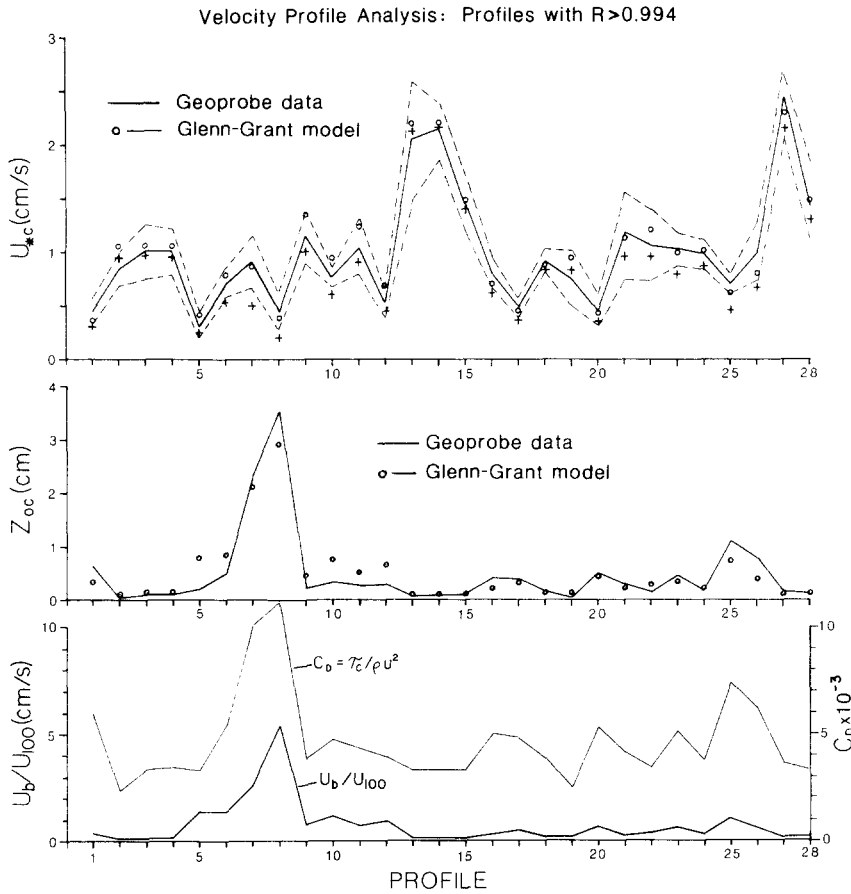


Fig. 7. Shear velocity (U_{*c}) and roughness length (z_{oc}) values derived from the log velocity profile method using only profiles for which $R^2 \cong 0.994$. Refer to Table 2 for the time of each of the numbered profiles. Estimates from the data are presented as the solid lines and 90% confidence intervals on U_{*c} are shown as dashed lines. U_{*c} and z_{oc} values computed by the wave-current model are shown as open circles. The crosses in the top panel show U_{*c} estimates made using the constant boundary drag coefficient ($C_D = 3 \times 10^{-3}$) which is appropriate for a rough boundary without wave-induced oscillatory currents (STERNBERG, 1972). The lower panel presents the observed C_D along with the observed wave-current speed ratio, U_b/\bar{U}_{100} , where $U_b = U_{b1/10}$.

magnitude needed to explain the observed z_{oc} values. The dimensions of the required bedforms can be roughly estimated using the wave ripple roughness equation developed by GRANT and MADSEN (1982); $k_b \cong 28(h^2/L)$, and the further requirement that the length of the bedforms had to be larger than the field of view of the GEOPROBE bottom camera. Thus, for $k_b = 90$ cm and $\lambda = 1$ m, the required ripple height would have been about 18 cm. The development of bedforms of that size on a predominantly mud substrate (mean sediment diameter = $40 \mu\text{m}$) is extremely doubtful. Admitting this possibility for the sake of argument, the LED transmissometer data at 98 cm ab and the velocity profiles after the storm provide conclusive evidence against the growth of large ripples or mud waves. Specifically, the formation of wave ripples of height H from a flat bed would require the

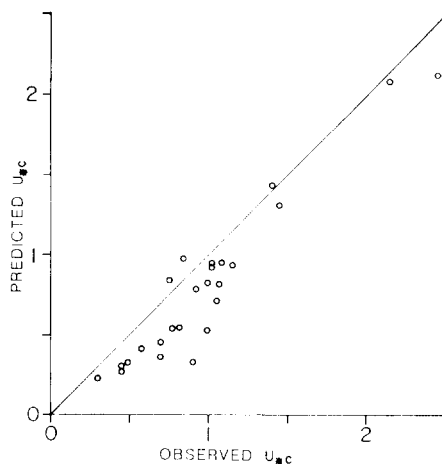


Fig. 9. Observed shear velocity (U_{*c}) versus the shear velocity calculated for a constant $z_o = 0.08$ cm (i.e. no wave-induced flow components). The data are for only those profiles that had $R^2 \cong 0.994$.

mobilization and reworking of a sediment layer of thickness $0.5H$. This process (for $H = 18$ cm) would have exposed many $g\text{ cm}^{-2}$ of sediment to the wave-current flow and would have generated a bottom turbid layer with SPM concentrations several orders of magnitude above the observed SPM concentration of $5\text{--}6\text{ mg l}^{-1}$. Moreover, the large bedforms would have had to degrade to nearly a flat bed within a few hours to explain the return to small z_{oc} values after the storm (Table 2). It is clear that ephemeral large bed roughness elements somewhere upstream of the GEOPROBE site cannot be invoked to explain the large observed z_{oc} , C_D , and U_{*c} values. Rather the response of the boundary layer to the wide variation in U_b/U_r values is exactly as expected in a combined

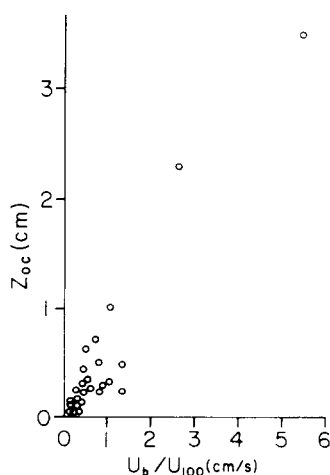


Fig. 10. The apparent roughness length (z_{oc}) for the current profiles having $R^2 \cong 0.994$ is shown to be a function of the relative strengths of the waves and currents, as predicted by the model of GRANT and MADSEN (1979).

wave-current flow over a rough seabed. As shown in Figs 7 and 10 there is a strong direct correlation between U_b/U_r and z_{oc} . The *apparent* roughness length felt by the current declined to about 0.08–0.1 cm when U_b/U_r was low (<0.5) and increased rapidly for $U_b/U_r > 2.0$. Inspection of Fig. 7 suggests that the usual rough boundary C_D (3×10^{-3}) would provide an adequate estimate of U_{*c} when $U_b/U_r < 0.5$.

Combined-flow model predictions

The observed boundary layer adjustments to variations in wave and current amplitudes are qualitatively predicted by the combined-flow theory. In this section we will compare the observations on the flow and the bed response (i.e. wave ripples and sediment resuspension) to the predictions of the models of GRANT and MADSEN (1979; 1982) and GLENN and GRANT (1987) (hereafter GG87). We will examine the accuracy of U_{*c} and z_{oc} model results using different surface wave characterizations ($H_{1/3}$ and $H_{1/10}$) in the hope of shedding light on an issue that is important to sediment transport predictions, and we will briefly compare our sediment response measurements to the predictions of wave ripples by GM82 and suspended sediment by GG87.

The combined-flow model has been described in detail in GM79, in GRANT *et al.* (1984) and GLENN (1983). We will not repeat that description here. Briefly, the differing time scales of wave-induced oscillation and quasi-steady, low-frequency currents result in very different boundary layer thicknesses with the wave boundary layer (δ_w) near the sea floor measured in centimeters and the current boundary layer above δ_w measured in meters. Nonlinear interaction of the two flows near a rough boundary produces an increased turbulence that increases the shear within the wave boundary layer and also causes an increased flow dissipation that is experienced by the current as an *apparent* roughness (z_{oc}) in excess of the roughness (z_o) due to physical bed roughness features. The model solution for the velocity profile above δ_w (which is our focus in this study) is

$$|U| = \frac{|U_{*c}|}{\kappa} \ln \left(\frac{z}{z_{oc}} \right), \quad z > \delta_w$$

and z_{oc} , the apparent roughness length due to both the wave-induced turbulence and the physical character of the bed, is given by GM79 as

$$\frac{z_{oc}}{z_o} = \left(\frac{|U_{*cw}| |A_b|}{|U_b| |\kappa_b|} \right)^\beta,$$

$$\beta = \left(1 - \frac{|U_{*c}| |U_b|}{|U_b| |U_{*cw}|} \right)$$

and $k_b = 30z_o$, U_{*cw} is the shear velocity inside the wave boundary layer, and $|A_b|$ is the wave excursion amplitude at the bed ($A_b = |U_b| \omega^{-1}$). GM79 adopts an iterative method to solve the model based on the observed values of $|U_r|$ at height z_r , $|U_b|$ and $|A_b|$ for the wave-induced velocity component, k_b ($\approx 30z_o$) for the physical bed roughness, and ϕ_c , the acute angle between the steady current and the oscillatory flow. If the combined bed shear stress exceeds the threshold shear stress for any of the grain size components in the bed, movement will occur, bedforms may be generated, and particles placed in suspension. GRANT and MADSEN (1982) present a model to estimate ripple heights and wavelengths and

Table 3. Apparent roughness from log profiles

| Burst hour | U_b/U_{18} (cm s^{-1}) | R^2 | U_{*c} (cm s^{-1}) | z_{oc} (cm) | k_b (cm) |
|---------------|--|-------|------------------------------------|------------------|---------------|
| 187 | 0.15 | 0.995 | 1.23 | 0.17 | 5.1 |
| 311 | 0.20 | 0.997 | 0.84 | 0.04 | 1.2 |
| 347 | 0.17 | 0.999 | 2.16 | 0.10 | 3.0 |
| 459 | 0.16 | 0.998 | 1.25 | 0.08 | 2.4 |
| 1233 | 0.20 | 0.999 | 1.39 | 0.07 | 2.1 |
| 1315 | 0.42 | 0.996 | 1.13 | 0.05 | 1.5 |

the resulting k_b as a function of sediment grain diameter D and the nature of the combined flow near the bed, and GLENN and GRANT (1987) have expanded the bbl model to include sediment resuspension as a function of D , and the appropriate shear velocities (U_{*c} and U_{*cw}) in the bbl. We have used the complete combined-flow bbl model which includes predictions of initial motion, bedform character, and the suspended sediment concentrations for up to seven size classes (GLENN, 1983).

All of the necessary data to run the model were provided by the GEOPROBE wave and current measurements. However, good estimates of the physical roughness length (k_b) are required for each of the velocity profiles used in this study. We used two methods to compute k_b . One method involves using the bottom photographs (Figs 3 and 8) to estimate heights (h) and spacings (L) of mounds and depressions created by the benthos. These data are then used in the equation suggested by GM82, $k_b = 28h^2/L$, to estimate an approximate k_b range. The second method, which is preferred but is not always possible, used the velocity profile method during times when the mean current was much larger than the wave oscillatory component and the current profile was highly logarithmic ($R^2 > 0.994$). Our earlier analysis and discussion of the bottom photographs *prior* to the storm of 22 December (Fig. 3) suggested a physical k_b of about 1.5–3.0 cm, using the k_b relation to GM82. This estimated range for k_b is very sensitive to the selected height of the roughness elements. The difficulty involved in accurately estimating h from photographs ensures that k_b computed in this way will be a very approximate value.

The results of the velocity profile estimates of z_{oc} for measurements when $U_b/U_{100} < 0.2$ (Table 2) suggest a k_b range of 1.3 to 2.8 cm ($z_o = 0.03$ – 0.09 cm), in agreement with the photograph estimate (Fig. 8). To add support to this k_b estimate, we have analysed the data for the entire deployment and found that the high current velocity profiles yield $z_o \approx 0.05$ – 0.15 cm whenever the current is subthreshold (Table 3) and photographs show that the bed roughness is being produced by benthic biota. We note that the average physical roughness found in the present study ($z_o \approx 0.08$ cm, $k_b = 2.6$ cm) is quite close to the z_o of 0.1 cm estimated by GRANT *et al.* (1984) over a similarly-bioturbated mud-rich substrate in the CODE study area off northern California.

Our procedure in comparing the observations to the model predictions has been to use the k_b estimated from the velocity profile method (Table 3) for the data before and after the storm period when the bed roughness was clearly dominated by randomly-distributed biologic mounds and holes (Fig. 3). During the storm the beam attenuation data and the bottom photographs demonstrate sediment transport and wave ripple formation (Figs 5 and 8). The ripples had average wavelengths of 7–10 cm and maximum heights of about

1 cm in the bottom photograph taken at 0800 hours on 22 December as the storm waned (Fig. 8b and Table 2). These dimensions suggest a maximum ripple-roughness k_b of order 3–4 cm.

Following the storm there was a rapid degradation of the wave ripples as the benthos again became the dominant control on bed roughness; thus, after 0800 hours on 22 December we have again used $k_b = 2.6$ cm ($z_o = 0.08$ cm) as the stationary bed roughness length for the model computations. The model computed the ripple dimensions and k_b during the storm.

Results of the model estimates of U_{*c} , z_{oc} , and ripple characteristics (using $D = 0.004$ cm, the modal grain size at the site) are given in Table 2 and plotted in Fig. 7 along with the observed U_{*c} , 90% confidence limits, and z_{oc} values derived from the velocity profile method. We present the model predictions when the alternative choices, $U_{b1/3}$ and $U_{b1/10}$, are used to characterize the surface wave motions in Table 2. Inspection of the U_{*c} predictions in Table 2 shows that either of the wave parameters yield satisfactory model results when the wave motions are relatively small (i.e. $U_b/U_r < 1$). However, enhancement of apparent roughness is a nonlinear function of wave intensity, and increases as U_b increases. Consequently, the predicted U_{*c} and z_{oc} values for the storm period, when the waves were much stronger than the steady flow, are more dependent on the wave parameter choice. For our dataset, the results during the storm are in slightly better agreement with the velocity profile observations when $U_{b1/10}$ is used in the GM79 model.

The important point to be stressed here is that the model provides good estimates of the current shear velocity and boundary roughness variations for a wide range of relative wave and current strengths over a well-determined physical boundary roughness. In addition, the GG87 model, with the waves characterized by $U_{b1/10}$, adequately predicted the timing of initial particle resuspension and yielded wave ripple dimensions that were in accord with bedforms observed in post-storm bottom photographs (Fig. 8). However, the model prediction of suspended matter concentration at the peak of the storm (Table 2) was in better agreement with the data when we used $U_{b1/3}$ to characterize the wave motion. A definite choice between these wave parameters is not clearly indicated by our data and this analysis. However, it seems reasonable to expect that the stresses produced by the largest waves in a given time interval will be responsible for initial sediment motion and will determine bedform growth and dimensions. Moreover, the flow–bedform interaction is of such importance to the turbulent interaction near the bed that it is critical that the model properly describe the bedform production and geometry. Although the combined-flow models work equally well in predictions of the dynamical quantities outside the wave boundary layer when we use either $U_{b1/3}$ or $U_{b1/10}$, we conclude that the sediment response during transport events will be more accurately modelled with $U_{b1/10}$.

CONCLUSIONS

The field data we have presented are well suited to an examination of wave–current interaction and model predictions. Previous field studies have suffered to some extent from either a limited range of rather low current and wave speeds or uncertainty regarding the physical bed roughness. Without adequate information on bedforms the observed changes in z_{oc} and U_{*c} during transport events could be caused by bed roughness variation. The results and analysis of the present data support the following conclusions.

(1) Wave-enhancement of the bottom boundary roughness length is demonstrated by the observed velocity profiles during a winter storm when the U_b/U_r ratio was as large as 8.5. The wave ripples observed immediately after the storm were far too small to account for a measured z_{oc} of 2–3 cm ($k_b = 60$ –90 cm).

(2) Observed z_{oc} and C_D values were strongly related to the relative strengths of the waves and currents, precisely as predicted by combined-flow theory. $C_D (= \tau_c/\rho U_{100}^2)$ values ranged from about 3×10^{-3} when waves were small to 12×10^{-3} when the waves exceeded the mean current. The use of a constant $C_D = 3 \times 10^{-3}$ for rough bottom, steady flow would have led to significant underpredictions of the observed τ_c .

(3) The effects of wave and current interaction near a rough boundary composed of movable sediment were predicted well by the GM79 and GM82 models. With wave motion described as $U_{b1/10}$, the model accurately predicted the important dynamical parameters above the wave boundary layer and also adequately predicted initial motion, bedform growth, and ripple dimensions during the December storm event.

(4) Although the model predictions were excellent during nonstorm conditions when waves were characterized with $H_{1/3}$ and $U_{b1/3}$, the results began to deviate from observations during the interval of large waves and small currents. This issue is especially important for sediment erosion and transport computations because the bed shear stress varies with U_b^2 and also any underestimates of U_{*c} will have a large impact on the calculated vertical distribution of suspended matter in the entire bottom boundary layer. The boundary layer flow and sediment transport observations during storm conditions were predicted best when we used $H_{1/0}$ and $U_{b1/10}$ to characterize the waves. The magnitude of the effect that the wave-generated turbulence at the bed has upon the apparent bed roughness (z_{oc}) increases rapidly for $U_b/U_{100} > 2$ and for a sea floor covered by wave ripples. Below that value, it appears that either $H_{1/3}$ or $H_{1/10}$ will give acceptable model results for U_{*c} , z_{oc} and C_D .

Acknowledgements—We acquired the GEOPROBE data as a part of the California Monitoring Program (CAMP) funded by the Minerals Management Service of the U.S. Department of the Interior. The excellent work at sea and in the lab of G. Tate, J. Thede, J. Nicholson and R. Viall is gratefully acknowledged. Scott Glenn kindly made the boundary layer model available to us. We thank B. Butman, C. A. Butman and W. Strahle for help at sea. We thank H. A. Karl, P. L. Wiberg and two anonymous journal reviewers for many helpful comments. The Captain and crew of the USGS Ship R.V. *Farnella* were critical to the success of our field work.

REFERENCES

- BAKER E. T. and J. W. LAVELLE (1984) The effect of particle size on the light attenuation coefficient of natural suspensions. *Journal of Geophysical Research*, **89**, 8197–8203.
- BRETSCHNEIDER C. L. (1966) Wave generation by wind, deep and shallow water. In: *Estuary and coastline hydrodynamics*, A. T. IPPEN, editor, McGraw-Hill, New York, pp. 133–196.
- CACCHIONE D. A. and D. E. DRAKE (1979) A new instrument system to investigate sediment dynamics on continental shelves. *Marine Geology*, **30**, 299–312.
- CACCHIONE D. A. and D. E. DRAKE (1982) Measurements of storm-generated bottom stresses on the continental shelf. *Journal of Geophysical Research*, **87**, 1952–1961.
- CACCHIONE D. A. and D. E. DRAKE (1990) Shelf sediment transport. In: *The sea*, Vol. 10, B. LEMEHUET and D. HANES, editors, Wiley-Interscience, New York.
- CACCHIONE D. A., W. D. GRANT, D. E. DRAKE and S. M. GLENN (1987) Storm-dominated bottom boundary layer dynamics on the northern California continental shelf: Measurements and predictions. *Journal of Geophysical Research*, **92**, 1817–1827.

- DRAKE D. E. and D. A. CACCHIONE (1986) Field observations of bed shear stress and sediment resuspension on continental shelves, Alaska and California. *Continental Shelf Research*, **6**, 415–429.
- GLENN S. M. (1983) A continental shelf bottom boundary layer model: The effects of waves, currents, and a moveable bed. ScD thesis, Massachusetts Institute of Technology, Cambridge, 237 pp.
- GLENN S. M. and W. D. GRANT (1987) A suspended sediment stratification correction for combined wave and current flows. *Journal of Geophysical Research*, **92**, 8244–8264.
- GRANT W. D. and O. S. MADSEN (1979) Combined wave and current interaction with a rough bottom. *Journal of Geophysical Research*, **84**, 1797–1808.
- GRANT W. D. and O. S. MADSEN (1982) Moveable bed roughness in unsteady oscillatory flow. *Journal of Geophysical Research*, **87**, 469–481.
- GRANT W. D. and O. S. MADSEN (1986) The continental-shelf bottom boundary layer. *Annual Review of Fluid Mechanics*, **18**, 265–305.
- GRANT W. D., A. J. WILLIAMS and S. M. GLENN (1984) Bottom stress estimates and their prediction on northern California continental shelf during CODE-1: The importance of wave–current interaction. *Journal of Physical Oceanography*, **14**, 506–527.
- GREEN M. O., J. M. REES and N. D. PEARSON (1990) Evidence for the influence of wave–current interaction in a tidal boundary layer. *Journal of Geophysical Research*, **95**, 9629–9644.
- GROSS T. F. and A. R. M. NOWELL (1983) Mean flow and turbulence scaling in a tidal boundary layer. *Continental Shelf Research*, **2**, 109–126.
- HEATHERSHAW A. D. (1979) The turbulent structure of the bottom boundary layer in a tidal current. *Geophysical Journal of the Royal Astronomical Society*, **58**, 395–430.
- HUNTLEY D. A. and D. G. HAZEN (1988) Seabed stresses in combined wave and steady flow conditions on the Nova Scotia continental shelf. Field measurements and predictions. *Journal of Physical Oceanography*, **18**, 347–362.
- LARSEN L. H., R. W. STERNBERG, N. C. SHI, M. A. H. MARSDEN and L. THOMAS (1981) Field investigations of the threshold of grain motion by ocean waves and currents. *Marine Geology*, **42**, 105–132.
- LESHT B. M. (1980) Benthic boundary layer velocity profiles: Dependence on averaging periods. *Journal of Physical Oceanography*, **10**, 985–991.
- SMITH J. D. (1977) Modeling of sediment transport on continental shelves. In: *The Sea*. Vol. 6. Wiley-Interscience, New York, pp. 539–577.
- STERNBERG R. W. (1972) Predicting initial motion and bedload transport of sediment particles in the shallow marine environment. In: *Shelf sediment transport: process and pattern*, D. J. P. SWIFT, D. B. DUANE and O. H. PILKEY, editors, Dowden, Hutchinson and Ross, Stroudsburg, PA, pp. 61–82.
- WIBERG P. L. and J. D. SMITH (1983) A comparison of field data and theoretical models for wave–current interactions at the bed on the continental shelf. *Continental Shelf Research*, **2**, 147–162.